Impact of dynamical fermions on the center vortex gluon propagator

James C. Biddle, Waseem Kamleh, and Derek B. Leinweber

Centre for the Subatomic Structure of Matter, Department of Physics,
The University of Adelaide, SA 5005, Australia

The impact of $SU(3)$ center vortices on the Landau-gauge gluon propagator is calculated in the presence of dynamical fermions and compared to the pure Yang-Mills case. The presence of dynamical fermions is found to alter the behavior of the center vortex propagator when compared to the established pure-gauge result. The gluon spectral representation is also explored from the center vortex perspective, where center vortices are shown to exhibit clear signs of positivity violation, which is an indicator of confinement. Vortex removal subsequently restores positivity, demonstrating the crucial role center vortices play in the confinement of gluons.

I. INTRODUCTION

The first step in any lattice calculation is to simulate the ground state QCD fields that permeate the vacuum. These fields give rise to the fundamental QCD features of confinement and dynamical chiral symmetry breaking resulting in dynamical generation of mass. Naturally, there has been substantial effort from the community to deduce what aspect of these fields gives rise to these features. Techniques have been developed to identify topological defects such as Abelian monopoles [1,2], instantons [3–6] and center vortices [7–10] within these ground state fields that present possible answers to this question. Center vortices are of particular interest as they offer access to the most fundamental mechanism that could underpin these phenomena.

The center vortex picture of QCD has experienced a renewed interest in recent years due to a host of lattice results reinforcing their importance in an understanding of the nonperturbative properties of QCD. The majority of these studies have been performed in the context of pure-gauge QCD, where the effects of fermion loops are omitted from the lattice Monte Carlo procedure. These results have shown that vortex removal results in a loss of dynamical mass generation [11–13], loss of string tension [14,15] and the suppression of the infrared landau gauge gluon propagator [15,16]. Vortices alone have been capable of reproducing the qualitative picture of nonperturbative QCD through reproduction of the linear static quark potential

[14,17,18], an infrared dominated gluon propagator [16] and the reintroduction of dynamical mass generation in the low-lying hadron spectrum [13].

Despite the success of these results, there has been a persistent quantitative discrepancy between center-vortex results and those from the original gauge fields on which the vortices are identified. This manifests in a variety of ways, most notably in a lower string tension obtained from the static quark potential [14,17,18], lower hadron masses in the low-lying hadron spectrum [13] and in residual infrared strength being retained by the vortex-removed gluon propagator [16]. The origin of these discrepancies is as-yet unknown, but they suggest a common property present in existing vortex studies.

Recently, work has been done to examine the effect of dynamical fermions on the structure of center vortices and the corresponding impact on the static quark potential [19,20]. These results showed for the first time a quantitative agreement between vortex-only results and those obtained from unmodified gauge fields. These results motivate further exploration of the relationship between center vortices and dynamical fermions. Here we continue this line of investigation by calculating the Landau gauge gluon propagator on vortex-modified configurations in the presence of dynamical fermions.

We will also examine the gluon spectral density by calculating the Euclidean correlator to determine the presence or absence of positivity violation, as positivity violation serves as an indicator of gluon confinement [21]. It is well understood that positivity violation in the gluon and quark propagators is a necessary condition for light-quark confinement [22]. As such, positivity violation arising from center vortices serves as a strong indication that the center vortex mechanism underpins the confinement of physical particles.

This paper is structured as follows. Section II outlines the vortex identification procedure on the lattice and describes the ensembles used in this work. Section III introduces the gluon propagator and presents the results from our center-vortex studies. Section IV discusses the notion of positivity violation and presents results based on an examination of the Euclidean correlator. Section V will summarize the findings of this paper.

II. VORTEX IDENTIFICATION

The procedure of center vortex identification on the lattice is now well established [16,23]. To identify the "thin" lattice vortices that correspond to the center of physical "thick" vortices [24,25], it is necessary to bring all configurations in an ensemble into the maximal center gauge. This is done by applying a gauge transformation $\Omega(x)$ such that the functional

$$R = \frac{1}{VN_{\dim}n_c^2}\sum_{x,\mu}|\mathrm{Tr}U_\mu^\Omega(x)|^2, \qquad (1)$$

is maximized. This serves to bring every gauge link $U_\mu(x)$ as close as possible to a center element of $SU(3)$, where the group center is comprised of the three elements proportional to the identity

$$\mathbb{Z}_3 = \exp\left(m\frac{2\pi i}{3}\right)I, \qquad m \in \{-1, 0, +1\}. \qquad (2)$$

A more detailed description of the algorithm used to perform this updating procedure can be found in Ref. [19].

Once fixed to maximal center gauge, a new ensemble is constructed by projecting each link onto its nearest center element. This center-projected configuration is known as the vortex-only configuration, $Z_\mu(x)$. From this construction, we also define the vortex-removed ensemble as $R_\mu(x) = Z_\mu^\dagger(x)U_\mu(x)$. The result of this procedure is three ensembles:

(1) Original, untouched (UT) fields, $U_\mu(x)$.
(2) Vortex-only (VO) fields, $Z_\mu(x)$.
(3) Vortex-removed (VR) fields, $R_\mu(x)$.

We refer to the latter two collectively as the vortex-modified ensembles. It is these three ensembles that we study to determine the impact of center vortices.

For this work, we make use of three original (UT) ensembles of 200 $32^3 \times 64$ lattice gauge fields. Two of these are $(2+1)$ flavor dynamical ensembles from the PACS-CS collaboration [26]. The heaviest pion mass of 701 MeV and lightest pion mass of 156 MeV are chosen to provide the greatest range of masses to best see the impact of center vortices as the physical point is approached. The third ensemble is pure Yang Mills, and provides a reference point to previous studies. This pure-gauge ensemble has been tuned to have a similar lattice spacing as the

TABLE I. A summary of the lattice ensembles used in this work [26].

Type	a (fm)	β	$\kappa_{u,d}$	m_π (MeV)
Pure gauge	0.100	2.58	$\cdots$	$\cdots$
Dynamical	0.102	1.9	0.13700	701
Dynamical	0.093	1.9	0.13781	156

dynamical ensembles so that finite volume effects should be similar across all ensembles used in this work. A summary of the ensemble parameters is provided in Table I.

III. GLUON PROPAGATOR

A. Definition

In the continuum, the momentum-space Landau gauge gluon propagator is of the form

$$D_{\mu\nu}^{ab}(q) = \left(\delta_{\mu\nu} - \frac{q_\mu q_\nu}{q^2}\right)\delta^{ab}D(q^2), \qquad (3)$$

where $D(q^2)$ is the scalar gluon propagator. On the lattice, the scalar propagator for $p^2 \neq 0$ is calculated by considering [16]

$$D(p^2) = \frac{2}{3(n_c^2 - 1)V}\langle\mathrm{Tr}A_\mu(p)A_\mu(-p)\rangle, \qquad (4)$$

where $n_c = 3$ is the number of colors, V is the lattice volume and $A_\mu(p)$ is calculated via the discrete Fourier transform of the midpoint definition of the gauge potential [27],

$$A_\mu(x + \hat\mu/2) = \frac{1}{2i}(U_\mu(x) - U_\mu^\dagger(x))$$
$$- \frac{1}{6i}\mathrm{Tr}(U_\mu(x) - U_\mu^\dagger(x)) + \mathcal{O}(a^2). \quad (5)$$

As the gauge fields used in this analysis are generated using the $\mathcal{O}(a^2)$-improved Iwasaki action [28], the tree-level behavior of the gluon propagator is improved by making the substitution [29–31]

$$p_\mu \to q_\mu = \frac{2}{a}\sqrt{\sin^2\left(\frac{p_\mu a}{2}\right) + \frac{1}{3}\sin^4\left(\frac{p_\mu a}{2}\right)}, \quad (6)$$

where p_μ are the usual lattice momentum variables

$$p_\mu = \frac{2\pi n_\mu}{aN_\mu}, \qquad n_\mu \in \left(-\frac{N_\mu}{2}, \frac{N_\mu}{2}\right], \qquad (7)$$

and N_μ is the lattice extent in the μ direction. The tree-level continuum scalar propagator is then given by $D(q^2) = \frac{1}{q^2}$. This choice of momentum variables reduces the sensitivity

of the gluon propagator to finite lattice spacing effects at large momenta [32].

The perturbative scalar propagator is defined as $D(q^2) = \frac{Z(q^2)}{q^2}$. For the remainder of this section we will focus on the renormalization function $Z(q^2) = q^2 D(q^2)$. We then renormalize $Z(q^2)$ in the momentum space subtraction (MOM) scheme [33,34] on the untouched configurations by enforcing the condition that $Z^{UT}(\mu^2) = 1$ at the largest available momentum on all ensembles, $\mu = 5.5$ GeV. This is performed via determination of a constant Z_3^{UT} satisfying

$$\frac{Z_{bare}^{UT}(\mu^2)}{Z_3^{UT}} = Z^{UT}(\mu^2) = 1. \qquad (8)$$

Renormalizing the vortex-modified results requires more careful consideration, as there is no *a priori* method by which it should be performed. Specifically, the problem arises from the absence of a perturbative expectation for the vortex-only propagator. The vortex-removed results are expected to encapsulate the high-momentum behavior, and as such one can reasonably expect that the MOM scheme method would apply to these ensembles. However, the vortex-only results are dominated by infrared strength and a decay to 0 at high momentum. Hence, a multiplicative renormalization based on a perturbative expectation does not apply.

To approach this renormalization issue, we present two sets of results. The first set will display all propagators from an ensemble divided by Z_3^{UT} as determined via the MOM scheme described in Eq. (8). This allows us to readily compare the vortex-modified propagators across all ensembles.

Based on the findings of Ref. [16], we also consider renormalizing the vortex-modified propagators via a best-fit approach. To do this, we consider taking a linear combination of the vortex-only and vortex-removed bare renormalization functions, $Z_{bare}^{VO}(q^2)$ and $Z_{bare}^{VR}(q^2)$, respectively, such that the "reconstructed" propagator

$$Z^{recon}(q^2) = \frac{\zeta^{VO} Z_{bare}^{VO}(q^2) + \zeta^{VR} Z_{bare}^{VR}(q^2)}{Z_3^{UT}} \qquad (9)$$

is fit to $Z^{UT}(q^2)$ via a linear least-squares fit. Here, ζ^{VO} and ζ^{VR} are fit parameters defined such that the renormalized vortex-modified propagators are

$$Z^{VO}(q^2) = \frac{\zeta^{VO}}{Z_3^{UT}} Z_{bare}^{VO}(q^2), \qquad (10)$$

$$Z^{VR}(q^2) = \frac{\zeta^{VR}}{Z_3^{UT}} Z_{bare}^{VR}(q^2). \qquad (11)$$

Fitting the reconstructed propagator is subject to the constraint

$$Z^{recon}(\mu^2) = Z^{UT}(\mu^2) = 1, \qquad (12)$$

so that the MOM scheme is replicated in the fit. This reduces the fit to a single parameter, as we can constrain e.g., ζ^{VR} to be

$$\zeta^{VR} = \frac{Z_3^{UT} - \zeta^{VO} Z_{bare}^{VO}(\mu^2)}{Z_{bare}^{VR}(\mu^2)}. \qquad (13)$$

Once a fit is found, the renormalization defined in Eqs. (10) and (11) is applied such that the reconstructed propagator is simply given by the sum

$$Z^{recon}(q^2) = Z^{VO}(q^2) + Z^{VR}(q^2). \qquad (14)$$

As we shall see, this fitting approach is appealing as it produces excellent agreement between the pure-gauge untouched propagator and the reconstructed propagator as defined in Eq. (9).

B. Results

We first present the pure-gauge calculation of the scalar propagator, with all results renormalized using the untouched renormalization constant, Z_3^{UT}. The results from the three ensembles, UT, VO and VR are shown in Fig. 1. As expected, these results agree with those of Ref. [16], with the untouched propagator defined by an infrared peak and an ultraviolet plateau to tree level. The vortex-modified counterparts qualitatively capture these two features, with the vortex-only propagator featuring an infrared peak, whereas the vortex-removed results retain the ultraviolet plateau. However, there is still significant infrared strength
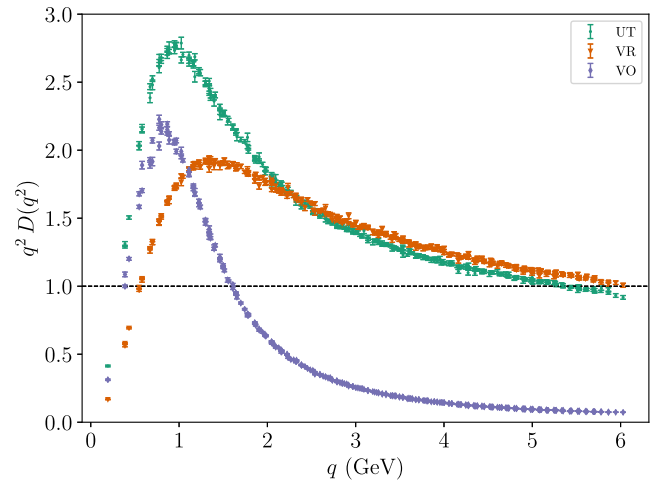
FIG. 1. Pure-gauge gluon propagator as calculated on the untouched (green), vortex-removed (orange) and vortex-only (purple) ensembles. All propagators a renormalized by applying the renormalization constant found by applying the MOM scheme to the untouched propagator. A black line at $Z(q^2) = 1$ is used to show the asymptotic behavior.

FIG. 2. $m_\pi = 701$ MeV gluon propagator. The data scheme is as described in Fig. 1.
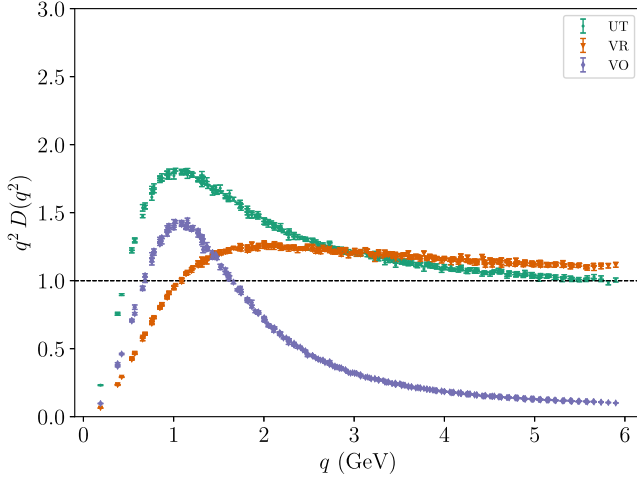
FIG. 3. $m_\pi = 156$ MeV gluon propagator. The data scheme is as described in Fig. 1.

present in the vortex-removed propagator, which indicates that some long-range physics remains in the vortex-removed ensemble.

We now consider the dynamical ensemble with the heaviest pion mass. We plot the gluon propagator calculated on this ensemble in Fig. 2. We observe that even at this unphysically large pion mass, the impact on the propagator is significant. Qualitatively, the propagators retain the same features as described for the pure-gauge sector; however the untouched propagator is noticeably screened, as is to be expected from the introduction of dynamical fermions [21]. The vortex-only propagator also exhibits screening, which is a heretofore unseen effect. Furthermore, the infrared enhancement of the vortex-removed propagator is significantly reduced when compared to the pure-gauge results shown in Fig. 1, and now displays behavior completely consistent with the perturbative expectation. These two changes indicate a noticeable shift in the behavior of the center vortices under the introduction of dynamical fermions.

The story is similar for the results of the lightest pion mass, shown in Fig. 3. Screening effects are further enhanced in the untouched propagator as the pion mass is reduced, although it is difficult to observe any change in screening in the vortex-only propagator. To aid in this, we plot a comparison of the vortex-only propagators across all three ensembles in Fig. 4. Here we can clearly see the presence of screening upon introduction of dynamical fermions. Between the two dynamical ensembles, screening effects are slightly enhanced as the pion mass decreases; however, the effect is very subtle. The vortex-removed propagator also retains the suppression of infrared enhancement found at $m_\pi = 701$ MeV. Given that the behavior of the vortex-modified propagators is so similar between the two pion masses, it appears that the mere presence of dynamical fermions plays a substantial role in
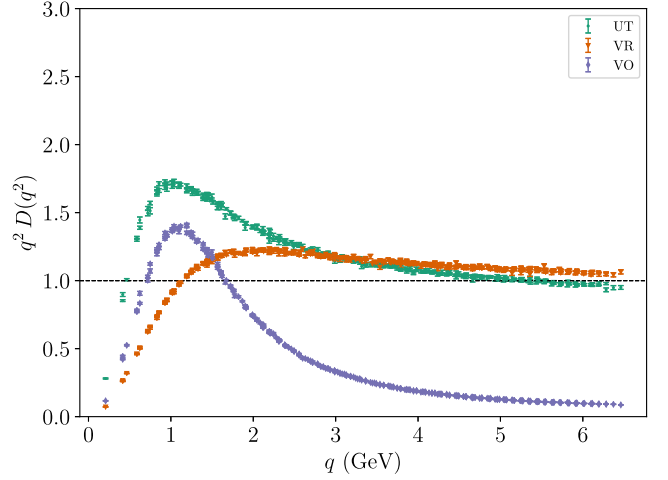
altering center vortex structure and the manner in which they generate the gluon propagator.

An interesting trend in the results presented in Figs. 1–3 is the fact that the vortex-removed results exceed the untouched results at high momentum with the same renormalization constant applied. It is well understood that a larger renormalization constant is necessary to account for increased roughness in an ensemble [35]. Given that the vortex removal process represents a significant change in the texture of the gauge field, it appears that such roughness has been induced in the vortex-removed fields. This finding supports the need for more detailed consideration of the renormalization of the vortex-modified propagators.

We now repeat the above presentation but with the second renormalization method applied, as defined at the end of Sec. III A. The pure-gauge results are presented in
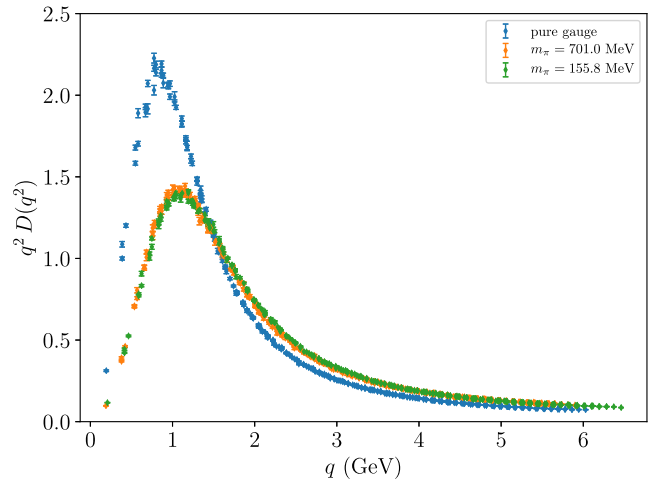
FIG. 4. The vortex-only propagators from all three ensembles. Screening is distinctly visible as we transition from pure-gauge to dynamical gauge fields.
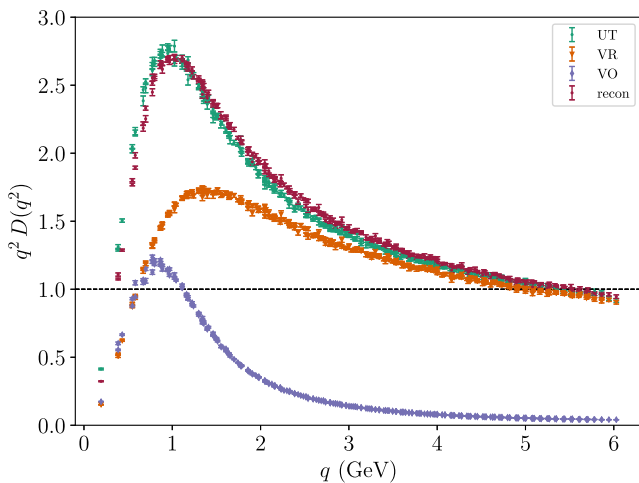
FIG. 5. Pure-gauge gluon propagator. All propagators are renormalized by applying the renormalization method described at the end of Sec. III A. The "recon" data (red) is an attempted reconstruction of the original propagator by summing the vortex-only and vortex-removed propagators.

Fig. 5. The shape of the propagators is naturally the same as before, with the interesting addition from the renormalization method being the reconstructed propagator. Here we observe good agreement between the untouched and reconstructed propagators. This indicates that the additional degree of freedom in the renormalization method is to some extent encapsulating the manner in which the untouched propagator is partitioned into its vortex-modified components.

The dynamical ensembles with this renormalization method applied, presented in Figs. 6 and 7, show a reduced agreement between the untouched and reconstructed propagators relative to the pure gauge results. The significance of this disagreement is unknown, and represents another interesting shift in behavior when transitioning from
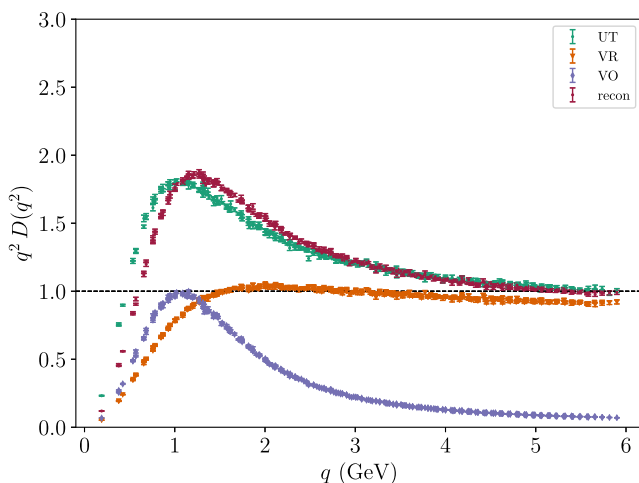
FIG. 6. $m_\pi = 701$ MeV gluon propagator. The data scheme is as described in Fig. 5.
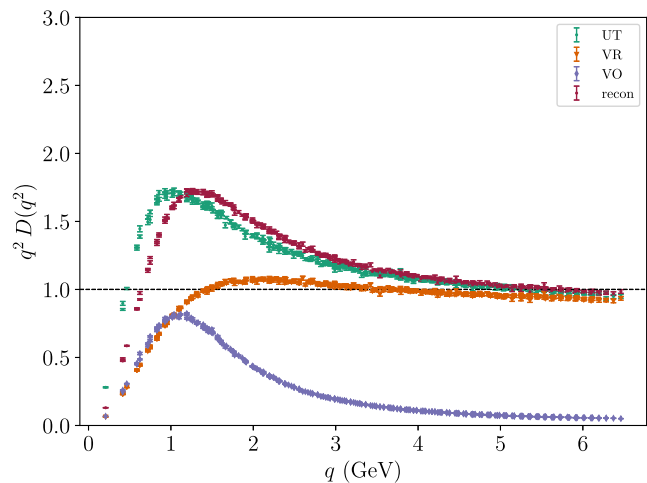
FIG. 7. $m_\pi = 156$ MeV gluon propagator. The data scheme is as described in Fig. 5.

pure-gauge to dynamical QCD. The fit constants as described in Eqs. (8) and (9) are presented in Table II.

When comparing the vortex-only propagators with this new renormalization scheme we observe that screening effects remain apparent, as is evident from Fig. 8. Furthermore, it is also possible to see a distinct increase in screening behavior as we transition from the heavy to light pion mass. This suggests that perhaps this renormalization method is more representative of the relative contributions of the vortex-only and vortex-removed propagators to the untouched propagator.

In summary, the vortex-modified propagators undergo significant changes in behavior upon the introduction of dynamical fermions. Residual infrared strength present in the pure-gauge vortex-removed propagator is suppressed in full QCD. The vortex-only propagators effectively capture screening effects manifesting as suppressed infrared enhancement, indicating that the long-range behavior of the vortex-only fields mirrors their untouched counterparts. Best-fit renormalization provides further insight into the structure of these vortex fields, where we find that the sum of vortex components reconstructs the original propagator to a fair degree. This further supports the idea that the vortex-only and vortex-removed propagators embody a splitting of the vacuum into long- and short-range strength, respectively.

TABLE II. The MOM scheme renormalization constants, Z_3^{UT}, as well as the fitted renormalization constants defined in Eq. (9).

Ensemble	Z_3^{UT}	ζ^{VO}	ζ^{VR}
Pure gauge	7.112	0.5543	0.8985
$m_\pi = 701$ MeV	9.316	0.6916	0.8251
$m_\pi = 156$ MeV	11.51	0.5834	0.8780
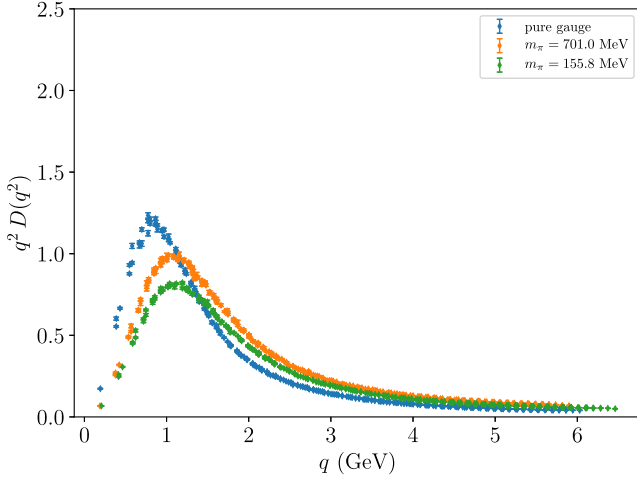
FIG. 8. The vortex-only propagators from all three ensembles. The best fit renormalization method produces a greater distinction between vortex-only propagators compared to Fig. 4.

IV. POSITIVITY VIOLATION

A. Discussion

For an arbitrary two-point function $D(x - y)$ to represent correlations between physical particles in the sense of a Wightman quantum field theory [36], it is necessary by the Osterwalder-Schrader axioms [37] for $D(x - y)$ to satisfy

$$\int d^4x\, d^4y\, f^*(-x_0, \mathbf{x}) D(x - y) f(y_0, \mathbf{y}) \geq 0, \quad (15)$$

for a suitable complex test function f. If this axiom is satisfied, then the scalar propagator defined in Eq. (4) has spectral representation

$$D(p^2) = \int_0^\infty dm^2 \frac{\rho(m^2)}{p^2 + m^2}, \quad (16)$$

with $\rho(m^2) \geq 0$, known as the Källen-Lehmann representation.

To investigate the behavior of the spectral representation, we consider the Euclidean correlator, $C(t)$, obtained by taking the Fourier transform of $D(p_0, \mathbf{0})$ as defined in Eq. (16) such that

$$C(t) = \frac{1}{2\pi} \int_{-\infty}^\infty dp_0 \int_0^\infty dm^2 \frac{\rho(m^2)}{p_0^2 + m^2} e^{-ip_0 t}. \quad (17)$$

Extending the p_0 integral to the complex plane and employing the residue theorem, one arrives at

$$C(t) = \int_0^\infty dm\, e^{-mt} \rho(m^2). \quad (18)$$

Clearly if $C(t) < 0$ for any t then $\rho(m^2)$ is not positive definite, and we say that positivity has been violated. This implies that there is no Källen-Lehmann representation as

defined in Eq. (16), and as such the propagator does not represent a correlation between physical states. Hence, the states do not appear in the physical spectrum. In the context of the gluon propagator, this can be taken as an indication that gluons are confined.

On the lattice [33], the Euclidean correlator, $C(t)$, is given by the discrete Fourier transform of the temporal component of Eq. (4),

$$C_{\text{lat}}(t) = \frac{1}{N_t} \sum_{n_t=0}^{N_t-1} e^{-2\pi i n t/N_t} D(q_4(n_t)^2), \quad (19)$$

where N_t is the lattice extent in the temporal direction and q_4 is the lattice momentum described in Eqs. (6) and (7). As $D(0)$ is associated with the lowest frequency mode of the propagator, it is a dominant term in Eq. (19). As such, it is essential to ensure that finite volume effects are accounted for.

On the lattice, finite volume effects alter the tensor structure of the propagator given in Eq. (3) such that it has the general form [33]

$$D_{\mu\nu}^{ab}(q) = \left(\delta_{\mu\nu} - \frac{h_{\mu\nu}(q)}{f(q^2)} \right) \delta^{ab} D(q^2), \quad (20)$$

where $f(q^2) \to q^2$ and $h_{\mu\nu} \to q_\mu q_\nu$ for large q_μ, but $f^{-1}(q^2)$ is finite at $q = 0$. We define

$$\tilde{h}_{\mu\nu}(q) = \frac{h_{\mu\nu}(q)}{f(q^2)}, \quad (21)$$

and note that in the infinite volume limit,

$$\begin{aligned} \tilde{h}_{\mu\mu}(q) &= f^{-1}(q^2) h_{\mu\mu}(q), \\ &= \frac{q_\mu q_\mu}{q^2}, \\ &= \frac{q^2}{q^2} \to 1 \quad \text{as } q^2 \to 0. \end{aligned}$$

However, on a finite volume lattice, $f^{-1}(q^2)$ cannot approach infinity. Since q_μ can take the value of 0 and $f^{-1}(q^2)|_{q^2=0}$ is finite, $\tilde{h}_{\mu\mu} = 0$ for $q_\mu = 0$ in a finite volume. Thus, the extraction of the scalar propagator $D(0)$ from the lattice propagator requires a normalization different from that of Eq. (4).

This change in normalization can be implemented by noting that the quantity

$$\left(\delta_{\mu\nu} - \frac{q_\mu q_\nu}{q^2} \right), \quad (22)$$

changes in the finite volume of the lattice to

$$(\delta_{\mu\nu} - \tilde{h}_{\mu\nu}(q)). \qquad (23)$$

For $q_\mu \neq 0$, setting $\mu = \nu$ and summing provides

$$\sum_\mu \left(\delta_{\mu\mu} - \frac{q_\mu q_\mu}{q^2} \right) = 4 - 1 = 3. \qquad (24)$$

But for $q_\mu = 0$ on the lattice, $\tilde{h}_{\mu\nu}(0) = 0$ and

$$\sum_\mu (\delta_{\mu\mu} - \tilde{h}_{\mu\mu}(q)) = 4. \qquad (25)$$

This results in

$$D_{\mu\mu}^{aa}(0) = 4(n_c^2 - 1)D(0), \qquad (26)$$

as opposed to

$$D_{\mu\mu}^{aa}(q) = 3(n_c^2 - 1)D(q), \qquad q \neq 0. \qquad (27)$$

To verify the validity of this factor we explore the behavior of the ratio of off-diagonal to diagonal propagator components for $q_\mu = 0$, i.e., ratios of the form

$$\frac{D_{\mu\nu}(0)}{D_{\rho\rho}(0)} = \frac{\tilde{h}_{\mu\nu}(0)}{1 - \tilde{h}_{\rho\rho}(0)}, \quad \mu \neq \nu, \qquad (28)$$

where ρ is not summed. As $\tilde{h}_{\mu\nu} \approx 0$, this ratio provides direct access to $\tilde{h}_{\mu\nu}$ relative to the Kronecker delta of 1.

The values of these ratios calculated on the pure-gauge untouched configurations are shown in Fig. 9. It is clear that these ratios are consistent with 0 at 1σ, indicating that both the diagonal and off-diagonal components of $\tilde{h}_{\mu\nu}$ are small relative to 1. These results are corroborated by the other ensembles used in this work. This determination justifies the use of a factor of 4 instead of 3 in calculating the scalar propagator at zero momentum to address the impact of the finite volume.
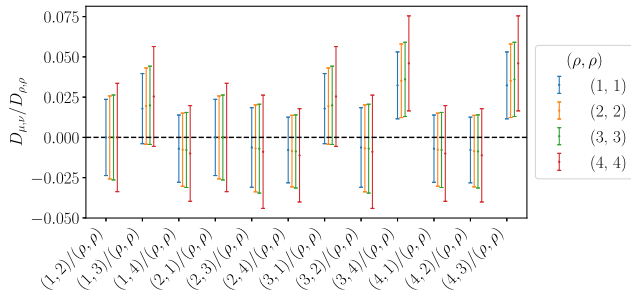
FIG. 9.   A plot of the 0-momentum ratio of the off-diagonal to diagonal tensor gluon propagator as described in Eq. (28). We observe that the majority of values are consistent with zero, indicating that the lattice correction function $\tilde{h}_{\mu\nu} \to 0$ as $q \to 0$.
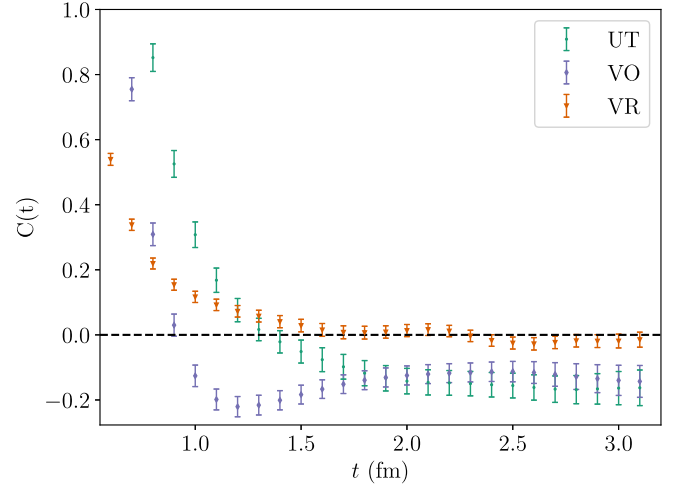
FIG. 10.   Pure-gauge Euclidean correlator. Shown are the results from the untouched (green), vortex-removed (orange) and vortex-only (purple) ensembles. A dashed line at $C(t) = 0$ is provided to aid in observing positivity violation.

B. Results

With this understanding developed, it is now possible to calculate $C(t)$ as defined in Eq. (19). The results for the pure-gauge ensembles are shown in Fig. 10. As expected [21], the untouched correlator shows clear signs of positivity violation. Interestingly, the vortex-only correlators also exhibit robust positivity violation. The positivity violation present in the vortex-removed result at large distances is consistent with the observations made in Fig. 1, where residual infrared strength in the vortex-removed gluon propagator is apparent. Thus, the separation of perturbative and nonperturbative physics through vortex modification is imperfect in the pure gauge sector.

The results from the dynamical ensembles, shown in Figs. 11 and 12 demonstrate an interesting change in
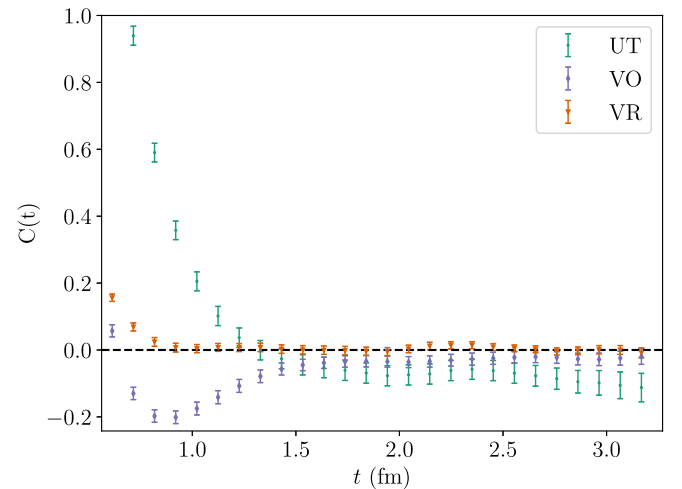
FIG. 11. $m_\pi = 701$ MeV Euclidean correlator. Data is as described in Fig. 10.
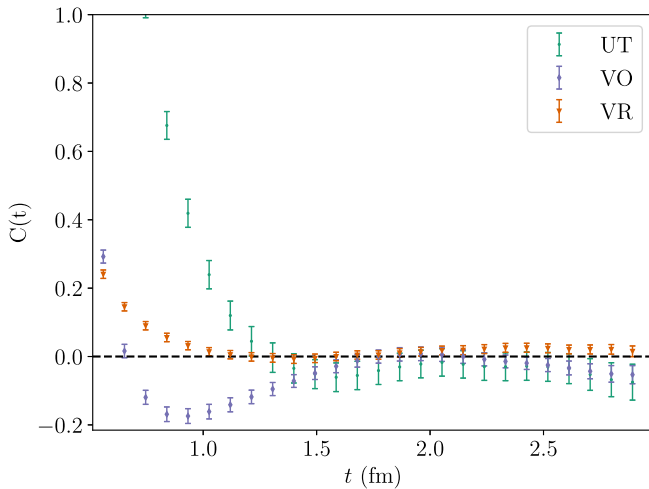
FIG. 12. $m_\pi = 156$ MeV Euclidean correlator. Data is as described in Fig. 10.

behavior. Here we observe a similar robust violation of positivity in the vortex-only results as observed on the pure-gauge ensemble. However, the untouched results show a lesser degree of positivity violation, especially on the lightest pion mass ensemble shown in Fig. 12. Note however that violation is still present at large times.

As with the gluon propagator results in the previous section, the most striking change is in the vortex-removed correlator. In this sector we now observe consistency with positivity. This supports the interpretation of the positivity violation in the vortex-removed pure-gauge results as being related to the residual nonperturbative infrared strength in the gluon propagator. As this residual strength is significantly diminished on the dynamical ensembles, we now see that the residual q^2 dependence in the VR renormalization function may be purely perturbative in origin. In this case, vortex modification has been successful in separating perturbative and nonperturbative physics.

In summary, vortex-only configurations exhibit significant positivity violation, as would be expected of a confining infrared-dominated theory. Conversely, the vortex removed configurations show a loss of this positivity violation, admitting the possibility that they do support a spectral representation of the propagator constructed from perturbative gluon interactions. These results provide additional support for the fact that center vortices encapsulate the confining aspects of QCD.

V. CONCLUSION

Calculations of the behavior of center vortices in the presence of dynamical fermions are new, and each

calculation provides further insight into the fascinating shift that center vortices appear to undergo upon the introduction of dynamical fermions. Here we have found that center vortices in the presence of dynamical fermions are effective in capturing the nonperturbative physics of QCD. Moreover, vortex removal appears to also be far more effective at removing the infrared strength of the propagator.

In regards to positivity violation, we establish the known result that unmodified lattice ensembles give rise to positivity violation in the Euclidean correlator [21]. We then determined that both with and without the presence of dynamical fermions there is clear evidence that vortex-only ensembles exhibit significant positivity violation. On our pure-gauge ensemble, the vortex-removed correlator showed slight positivity violation at long distances, but on both dynamical ensembles this effect vanished. In full QCD, center-vortex modification of the ground-state vacuum fields appears to provide an effective separation of perturbative and nonperturbative physics. These results present evidence that center vortices in the QCD ground-state vacuum fields provide the origin of confinement.

The results presented here add to the growing number of investigations into the impact of dynamical fermions on center vortices. We find marked differences between the pure-gauge and dynamical case, which implores further study. The origin of these disparities is currently unknown, and further work into the geometric structure of center vortices in full QCD is planned. It is clear that there is an intimate relationship between dynamical fermions and center vortices, and that this relationship has significant implications for the QCD vacuum.

[1] G. 't Hooft, Topology of the gauge condition and new confinement phases in non-Abelian gauge theories, Nucl. Phys. **B190**, 455 (1981).

[2] S. Mandelstam, Vortices and quark confinement in non-Abelian gauge theories, Phys. Rep. **23**, 245 (1976).

[3] A. A. Belavin, A. M. Polyakov, A. S. Schwartz, and Yu. S. Tyupkin, Pseudoparticle solutions of the Yang-Mills equations, Phys. Lett. **59B**, 85 (1975).

[4] E. Witten, Instantons, the quark model, and the 1/n expansion, Nucl. Phys. **B149**, 285 (1979).

[5] C. G. Callan, Jr., R. F. Dashen, and D. J. Gross, Toward a theory of the strong interactions, Phys. Rev. D **17**, 2717 (1978).

[6] Y. Aharonov, A. Casher, and S. Yankielowicz, Instantons and confinement, Nucl. Phys. **B146**, 256 (1978).

[7] G. 't Hooft, On the phase transition towards permanent quark confinement, Nucl. Phys. **B138**, 1 (1978).

[8] G. 't Hooft, A property of electric and magnetic flux in non-Abelian gauge theories, Nucl. Phys. **B153**, 141 (1979).

[9] J. M. Cornwall, Quark confinement and vortices in massive gauge invariant QCD, Nucl. Phys. **B157**, 392 (1979).

[10] H. B. Nielsen and P. Olesen, A quantum liquid model for the QCD vacuum: Gauge and rotational invariance of domained and quantized homogeneous color fields, Nucl. Phys. **B160**, 380 (1979).

[11] D. Trewartha, W. Kamleh, and D. Leinweber, Evidence that centre vortices underpin dynamical chiral symmetry breaking in SU(3) gauge theory, Phys. Lett. B **747**, 373 (2015).

[12] E.-A. O'Malley, W. Kamleh, D. Leinweber, and P. Moran, SU(3) centre vortices underpin confinement and dynamical chiral symmetry breaking, Phys. Rev. D **86**, 054503 (2012).

[13] D. Trewartha, W. Kamleh, and D. B. Leinweber, Centre vortex removal restores chiral symmetry, J. Phys. G **44**, 125002 (2017).

[14] K. Langfeld, Vortex structures in pure SU(3) lattice gauge theory, Phys. Rev. D **69**, 014503 (2004).

[15] P. O. Bowman, K. Langfeld, D. B. Leinweber, A. Sternbeck, L. von Smekal, and A. G. Williams, Role of center vortices in chiral symmetry breaking in SU(3) gauge theory, Phys. Rev. D **84**, 034501 (2011).

[16] J. C. Biddle, W. Kamleh, and D. B. Leinweber, Gluon propagator on a center-vortex background, Phys. Rev. D **98**, 094504 (2018).

[17] A. O'Cais, W. Kamleh, K. Langfeld, B. Lasscock, D. Leinweber, P. Moran, A. Sternbeck, and L. von Smekal, Preconditioning maximal center gauge with stout link smearing in SU(3), Phys. Rev. D **82**, 114512 (2010).

[18] A. Trewartha, W. Kamleh, and D. Leinweber, Connection between center vortices and instantons through gauge-field smoothing, Phys. Rev. D **92**, 074507 (2015).

[19] J. Biddle, W. Kamleh, and D. Leinweber, Static quark potential from centre vortices in the presence of dynamical fermions, arXiv:2206.00844.

[20] A. Virgili, W. Kamleh, and D. Leinweber, Smoothing algorithms for projected center-vortex gauge fields, arXiv:2203.09764 [Phys. Rev. D (to be published)].

[21] P. O. Bowman, U. M. Heller, D. B. Leinweber, M. B. Parappilly, A. Sternbeck, L. von Smekal, A. G. Williams, and J.-b. Zhang, Scaling behavior and positivity violation of the gluon propagator in full QCD, Phys. Rev. D **76**, 094505 (2007).

[22] C. D. Roberts, M. S. Bhagwat, A. Holl, and S. V. Wright, Aspects of hadron physics, Eur. Phys. J. Special Topics **140**, 53 (2007).

[23] J. C. Biddle, W. Kamleh, and D. B. Leinweber, Visualization of center vortex structure, Phys. Rev. D **102**, 034504 (2020).

[24] M. Engelhardt and H. Reinhardt, Center projection vortices in continuum Yang-Mills theory, Nucl. Phys. **B567**, 249 (2000).

[25] R. Bertle, M. Faber, J. Greensite, and S. Olejnik, Center vortices and color confinement in lattice QCD, arXiv:hep-lat/0009017.

[26] S. Aoki *et al.* (PACS-CS Collaboration), 2 + 1 flavor lattice QCD toward the physical point, Phys. Rev. D **79**, 034503 (2009).

[27] B. Alles, D. Henty, H. Panagopoulos, C. Parrinello, C. Pittori, and D. G. Richards, α_s from the nonperturbatively renormalised lattice three gluon vertex, Nucl. Phys. **B502**, 325 (1997).

[28] Y. Iwasaki, Renormalization group analysis of lattice theories and improved lattice action. II. Four-dimensional non-Abelian SU(N) gauge model, arXiv:1111.7054.

[29] K. Symanzik, Continuum limit and improved action in lattice theories. 1. Principles and ϕ^4 theory, Nucl. Phys. **B226**, 187 (1983).

[30] P. Weisz and R. Wohlert, Continuum limit improved lattice action for pure Yang-Mills theory. 2., Nucl. Phys. **B236**, 397 (1984); Erratum, Nucl. Phys. **B247**, 544 (1984).

[31] P. Weisz, Continuum limit improved lattice action for pure Yang-Mills theory. 1., Nucl. Phys. **B212**, 1 (1983).

[32] F. D. R. Bonnet, P. O. Bowman, D. B. Leinweber, A. G. Williams, and J. M. Zanotti, Infinite volume and continuum limits of the Landau gauge gluon propagator, Phys. Rev. D **64**, 034501 (2001).

[33] D. B. Leinweber, J. I. Skullerud, A. G. Williams, and C. Parrinello (UKQCD Collaboration), Asymptotic scaling and infrared behavior of the gluon propagator, Phys. Rev. D **60**, 094507 (1999); Erratum, Phys. Rev. D **61**, 079901 (2000).

[34] P. O. Bowman, U. M. Heller, D. B. Leinweber, M. B. Parappilly, and A. G. Williams, Unquenched gluon propagator in Landau gauge, Phys. Rev. D **70**, 034509 (2004).

[35] P. O. Bowman, U. M. Heller, D. B. Leinweber, and A. G. Williams, Gluon propagator on coarse lattices in Laplacian gauges, Phys. Rev. D **66**, 074505 (2002).

[36] A. S. Wightman, Quantum field theory in terms of vacuum expectation values, Phys. Rev. **101**, 860 (1956).

[37] K. Osterwalder and R. Schrader, Axioms for Euclidean Green's functions, Commun. Math. Phys. **31**, 83 (1973).